Dynamics Modeling and Tension Control of Composites Winding System Based on ASMC

QI HONG[ID], YAOYAO SHI, AND ZHEN CHEN

School of Mechanical Engineering, Northwestern Polytechnical University, Xi'an 710072, China

Corresponding author: Qi Hong (407460979@qq.com)

ABSTRACT Tension is a key processing parameter in the process of composite fiber tape winding. The fluctuation of tension will affect the accuracy of winding and the performance of winding products, such as stress uniformity, fatigue resistance, strength, compactness and resin content. In view of the winding tension is time-varying and the application of tension needs to be more accurate, a tension calculation model is established. Due to the influence of dynamic performance of tension control system by cogging torque, inverter dead zone, ring gear clearance, friction torque, parameter drift, and measurement noise, an adaptive sliding mode control (ASMC) based on extended state observer (ESO) is proposed. The stability of the closed-loop system is proven by Lyapunov theory, the system state variables is estimated by ESO, and the input dead-zone is compensated by the designed adaptive law. Simulation and experimental results show that ESO-based ASMC improves the robustness and dynamic response performance of the tension control system, and can effectively suppress the chattering of the sliding mode control system. The void content and residual stress of composite products have been improved obviously.

INDEX TERMS Composites tape winding, dynamics modeling, ESO, ASMC, tension control.

I. INTRODUCTION

Due to the rapid development of military and civil industries, especially advanced technologies such as aerospace and aviation, some materials with superior performance are needed. The traditional single material is difficult to meet the demand in strength, toughness, weight and stability. Composite materials can make up for many defects of metal materials in performance [1]–[5]. Composite winding products have been widely used in missile shell, rocket booster nozzle and pressure vessel. Winding forming is a common method in composite material forming process, and winding tension is an important parameter in composite material winding forming. Improper selection or control of tension during forming will lead to the lateral deviation and overhead of fiber belt on the forming surface, which will seriously affect the product quality [6]–[9].

The precise tension control system of filament winding is a nonlinear system with disturbance. It is difficult to realize the precise tension control by using the traditional control strategy. At present, researchers pay more and more attention to the research of winding tension, especially in

The associate editor coordinating the review of this manuscript and approving it for publication was Nishant Unnikrishnan.
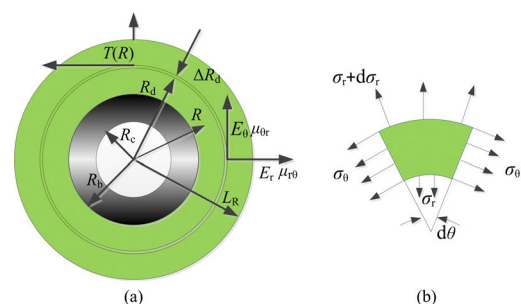

FIGURE 1. Cross section of winding products.

the control strategy of winding tension. In literature [10], a robust control algorithm based on disturbance observer for tension control system of cylinder winding equipment is proposed. The signal processing method based on vibration controller and observation sensor is designed to suppress the noise signal of the sensor. In literature [11], an winding tension model is established, and the fuzzy neural network PID controller is used to adjust the winding speed in real time. Because in the process of producing film under constant tension, the product is prone to wrinkle and end-face unevenness. In literature [12], a nonlinear time-varying
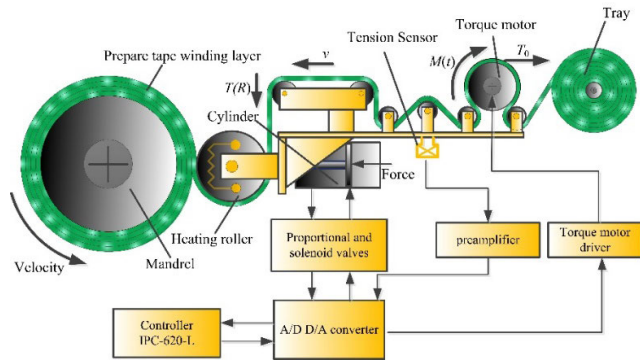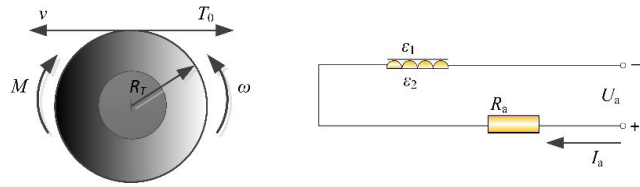
FIGURE 2. Tension control process.

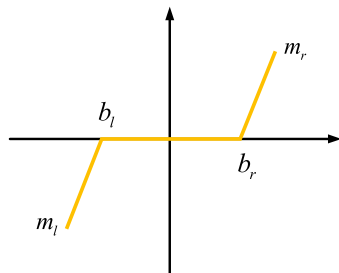**FIGURE 3. The process of tension produced by torque motor.**
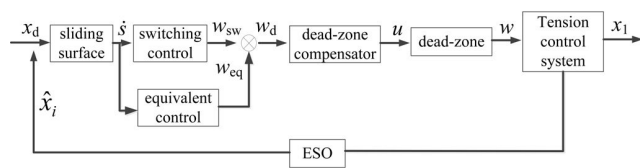

FIGURE 4. Dead-zone function.

FIGURE 5. Block diagram of the controller.

FIGURE 6. Step response of traditional PID (simulation).
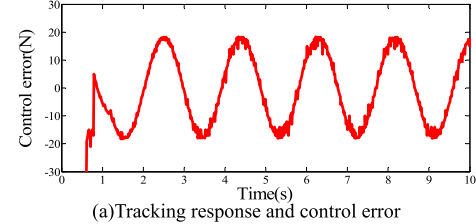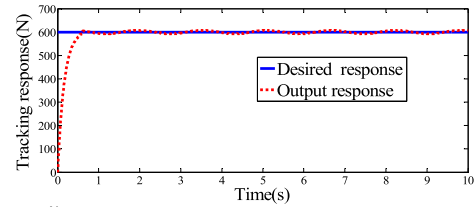
two-input and two-output model of the composite prepreg transport system was established based on the automated tape head. The synergetic decoupling control of transport speed and tension was performed combining with PI (proportional-integral) and diagonal matrix decoupling control algorithm. In literature **[13]**, a closed-loop control method of tensionless sensor with adaptive PI parameters is proposed. During the winding process, the measurement of tension by the tension sensor causes a measurement delay. A tension observer is designed to replace the tension sensor, and the tension observed value is used as feedback to realize the closed-loop control of the winding system. In literature **[14]**, for multi-parameter winding control system, a sliding mode feedback

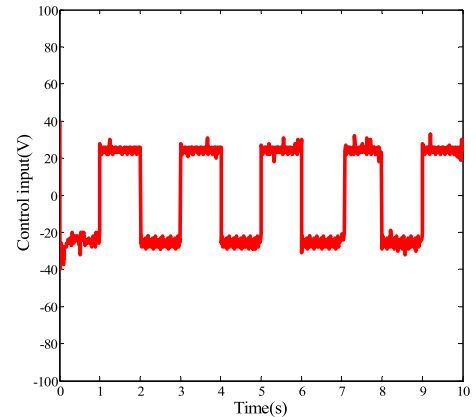linearization control algorithm is designed. In the case of coupling of winding tension and speed, the accuracy and stability of the control system are reduced, and the uncertainty of the system is increased. An ideal feedback linearisation control algorithm is used to decouple the tension and speed, which is composed of sliding mode speed controller and sliding mode tension controller. In literature **[15]**, the winding equipment of three-motor is composed of several control subsystems, which interfere with each other. A decentralized coordinated control algorithm is designed to reduce the interferences between subsystems. The observer is designed to replace the tension sensor according to the control system dynamics, core radius and rotation inertia. In literature **[16]**, an observer based feedback control method is proposed to reduce the increase of tension. The angular velocity is used to calculate the roll inertia. It is proved that when the system is started, the tension increases due to the influence of winding inertia. In literature **[17]**, an H∞ robust control strategy is proposed to solve the coupling of line tension and speed. Because The interference from the interference source in the velocity will be transmitted to the tension in the winding process. In literature **[18]**, according to the characteristics of filament tape winding process, the mathematical model of discontinuous winding and variable tension control system is established, and the adaptive controller is designed on the basis of classical PID control and fuzzy control. The results
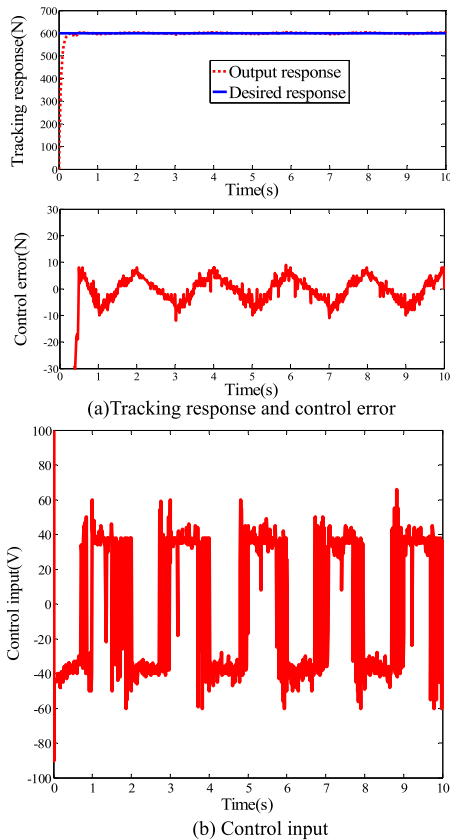
FIGURE 7. Step response of SMC with sgn(s) (simulation).

FIGURE 8. Step response of SMC with sat(s) ($\delta = 0.02$) (simulation).

show that the mathematical model has good reliability. The control method can be realized in the winding process and can ensure the tight adhesion of the fiber tape.

Due to the nonlinearity, poor parameter regulation and strong disturbance of the system, it is difficult for PID controller to achieve ideal control effect [19]–[22]. Sliding mode control has strong robustness and good control effect on nonlinear system. However, the high frequency buffeting of sliding mode control affects the system structure, damages the sensors and excites the unmodeled dynamics of the system [23]–[27]. Approach law and boundary layer method are used to reduce chattering, but the control accuracy is reduced [28]–[30]. In recent years, many scholars applies intelligent control technology to engineering practice. In literature [31], an adaptive linear neuron neural network is introduced into the traditional sliding mode observer, which has good performance. In order to reduce chattering in real time, an adaptive fuzzy logic is designed to Approach the parameters of the sliding mode controller [32]. In literature [33], combining internal model control and inverse system method is proposed, which can effectively improve the dynamic performance and control accuracy of bearingless permanent magnet synchronous motor. In literature [34], a speed observation based on artificial neural network inverse method is proposed, which can reduce the influence of speed detection on the accuracy and stability of bearingless induction motor
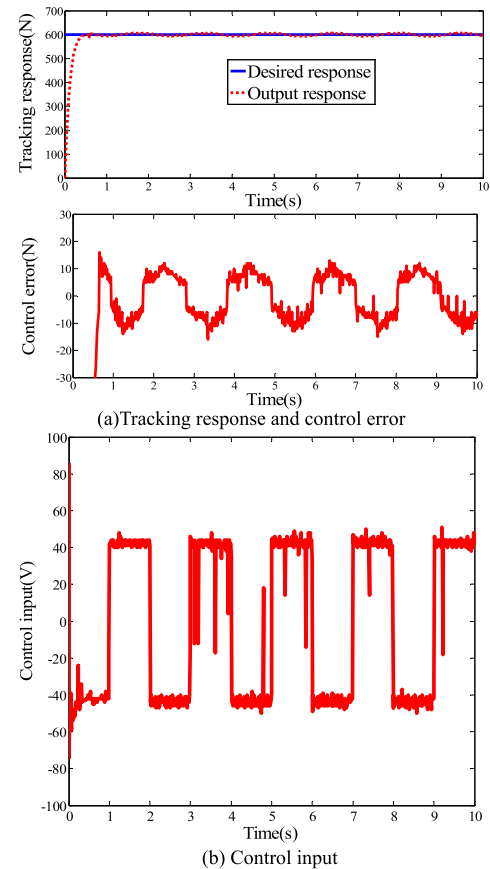
system. In literature [35], in order to improve the driving capability of permanent magnet synchronous wheel motor, combining the state feedback control method and the gray wolf optimization algorithm is proposed.

In this paper, the ESO-based SMC is used to improve the control accuracy of the tension control system of the winding equipment. Due to SMC algorithm has many advantages, such as no need for on-line system identification, insensitivity to parameter changes and disturbances, rapid response, easily applied to engineering, which is widely used in motor servo control system. The output variables of the control system is observed by ESO, and meanwhile, derivation of output variables is used to design sliding mode control law; finally, the parameter model of the input dead-zone is estimated by the designed adaptive law. The simulation and experiment show that the designed algorithm is reliable and effective, and winding products are also more superior in performance.

II. MATHEMATICAL MODEL OF TENSION CALCULATION
The cross-section of a single toroidal winding product is shown in **Fig. 1**. The winding is carried out on the core mould continuously, and the thickness of each individual winding layer is very small compared with the thickness of the product. Micro-body can be regarded as Orthotropic
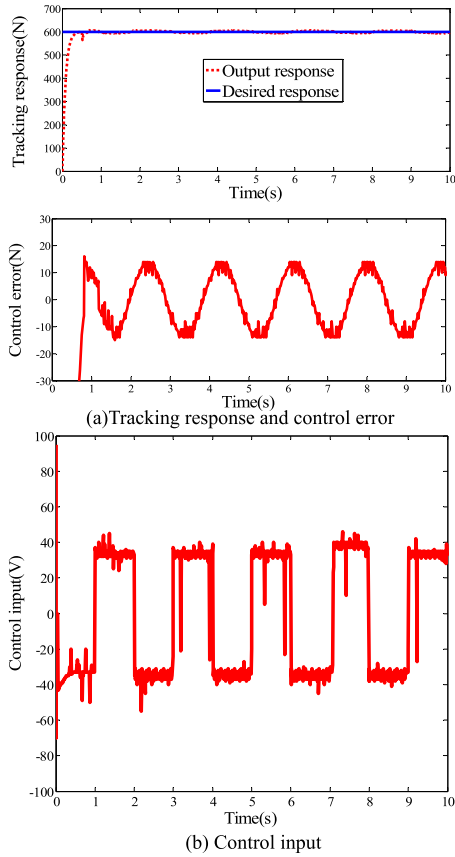
FIGURE 9. Step response of SMC with sat(s) ($\delta = 0.05$) (simulation).

FIGURE 10. Step response of ASMC (simulation).

Bodies, which is a essentially plane problem and can be solved by elastic theory.

From the equilibrium relation of the radial micro-body in Fig.1, the static equilibrium equation can be obtained as shown in (1).

$$(\sigma_r + d\sigma_r)(R + dR)\, d\theta - \sigma_r R d\theta - 2\sigma_\theta dR \sin\frac{d\theta}{2} = 0 \quad (1)$$

Higher order infinitesimal terms can be omitted, thus eq.1can be simplified into (2).

$$R\frac{d\sigma_r}{dR} + \sigma_r - \sigma_\theta = 0 \quad (2)$$

Boundary conditions of micro-body can be expressed as follows:

$$\begin{cases} \sigma_r(R_d, R_d) = 0 \\ \sigma_r(R_d, R_b) = -q(R_d) \\ \sigma_\theta(R_d, R_d) = T(R_d) \\ u(R_d, R_d) = 0 \end{cases} \quad (3)$$

where T is winding tension, R is the analyzed micro-body radius, θ is circumferential angle of micro-body. When the outer fiber tape is winding to the radius R_d, the pressure acting on the surface of the core mould is expressed as $q(R_d)$, $u(R_d, R_d)$ is radial displacement, $\sigma_r(R_d, R_d)$ is radial stress and $\sigma_\theta(R_d, R_d)$ is circumferential stress.
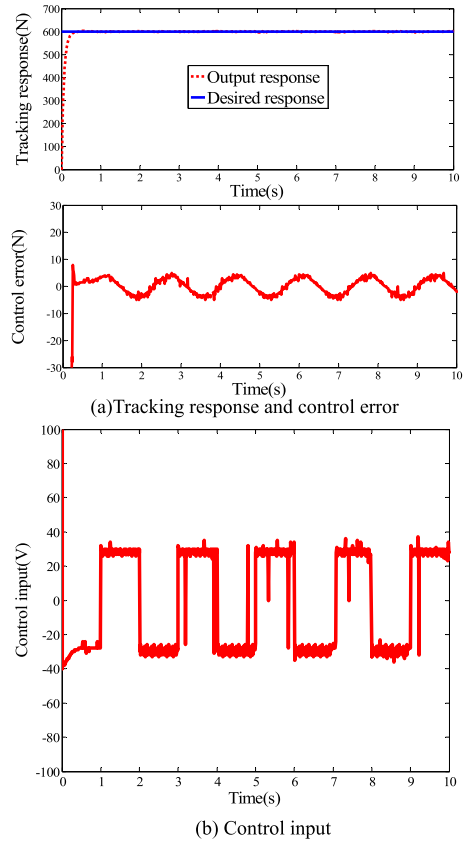
When the thickness of winding layer is ΔR_d, the stress and displacement can be rewritten as follows.

$$\begin{cases} \overline{\sigma_r}(R_d, R) = \sigma_r(R_d, R) + \Delta\sigma_r(R_d, R) \\ \overline{\sigma_\theta}(R_d, R) = \sigma_\theta(R_d, R) + \Delta\sigma_\theta(R_d, R) \\ \overline{u}(R_d, R) = u(R_d, R) + \Delta u(R_d, R) \end{cases} \quad (4)$$

The boundary conditions can be expressed as follows:

$$\begin{cases} \overline{\sigma_r}(R_d, R_d) = \Delta\sigma_r(R_d, R_d) = \dfrac{T(R_d)\Delta R_d}{R_d} \\ \overline{\sigma_r}(R_d, R_b) = \sigma_r(R_d, R_b) + \Delta\sigma_r(R_d, R_b) = -q - \Delta q \end{cases} \quad (5)$$

By substituting (4) into (2), a new equilibrium equation is obtained as follows:

$$R\frac{d\Delta\sigma_r}{dR} + \Delta\sigma_r - \Delta\sigma_\theta = 0 \quad (6)$$

The generalized Hooke's law expressed by displacement can be described as (7).

$$\begin{cases} \Delta\sigma_r = \dfrac{E_r G^2}{G^2 - E_r E_\theta}\left(\dfrac{d\,\Delta u}{dR} + \dfrac{E_r}{G}\dfrac{\Delta u}{R}\right) \\ \Delta\sigma_\theta = \dfrac{E_r G^2}{G^2 - E_r E_\theta}\left(\dfrac{\Delta u}{R} + \dfrac{E_r}{G}\dfrac{d\,\Delta u}{dR}\right) \\ G = \dfrac{E_\theta}{\mu_\theta} = \dfrac{E_r}{\mu_{r\theta}} \end{cases} \quad (7)$$

Substitute (7) into (6), then

$$\begin{cases} R^2 \dfrac{d^2 \Delta u}{dR^2} + R \dfrac{d\Delta u}{dR} - n^2 \Delta u = 0 \\ n = \sqrt{\dfrac{E_\theta}{E_r}}; \end{cases} \tag{8}$$

The solution of (8) can be expressed as follows:

$$\Delta u = g_1 R^n + g_2 R^{-n} \tag{9}$$

The following boundary conditions can be obtained.

$$\begin{cases} R = R_b \\ \Delta\sigma_R(R_d, R_b) = -\Delta q(R_d) \\ R = R_d \\ \Delta\sigma_R(R_d, R_d) = -\dfrac{T(R_d)\Delta R_d}{R_d} \end{cases} \tag{10}$$

Substitute (10) into (7), then

$$\begin{cases} \Delta u = \dfrac{G^2 - E_r E_\theta}{E_r G^2 (R_d^{2n} - R_b^{2n})} \\ \quad \times \begin{bmatrix} \dfrac{R_b^{n+1}\Delta q - T(R_d)R_d^n \Delta q}{X - N}R^n + \\ \dfrac{R_b^{2n}R_d^n(R_b R_d^n \Delta q - R_b^n T(R_d)\Delta q)}{Y + X}R^{-n} \end{bmatrix} \\ N = \dfrac{E_\theta}{E^m(R_b^2 - R_c^2)}\left[(1 - \mu^m)R_b^2 + (1 + \mu^m)R_c^2\right]; \\ Y = n - \dfrac{E_\theta}{G} - N; \\ X = n + \dfrac{E_\theta}{G} + N \end{cases} \tag{11}$$

where E is the elastic modulus of the product, μ is the poisson coefficient of the product, and m is the core mould.

Based on the thick wall theory in mechanics of materials, the radial displacement and stress of core mould can be expressed as (12).

$$\begin{cases} u^m(R_d, R) = \dfrac{R_b^2 q(R_d)}{E^m(R_b^2 - R_c^2)}\left[(1 - \mu^m)R + (1 + \mu^m)\dfrac{R_c^2}{R}\right] \\ \sigma_r^m(R_d, R) = \dfrac{R_b^2 q(R_d)}{(R_b^2 - R_c^2)}\left[1 - \dfrac{R_c^2}{R}\right] \\ \sigma_\theta^m(R_d, R) = \dfrac{R_b^2 q(R_d)}{(R_b^2 - R_c^2)}\left[1 + \dfrac{R_c^2}{R}\right] \end{cases} \tag{12}$$

The displacement continuity condition at boundary $R = R_b$ can be expressed as follows:

$$\Delta u(R_d, R_b) = \Delta u^m(R_d, R_b) = -\dfrac{R_b N}{E_r}\Delta q(R_d) \tag{13}$$

(14) can be derived from (11) and (13).

$$\Delta q = \dfrac{2nT(R_d)R_d^n R_b^{n-1}}{XR_d^{2n} + YR_b^{2n}} \tag{14}$$

Substitute (14) into (11), then

$$\Delta u = \dfrac{R_b^n R_d T(R_d)}{E_\theta(XR_d^{2n} + YR_d^{2n})} \\ \times \left[Y(X - N)(\dfrac{R_b}{R})^n - X(Y + X)(\dfrac{R}{R_b})^n\right] \tag{15}$$

When the final radius of the winding product is $R_d = L_R$, Q is the total pressure on the core mould surface that can be calculated by (16).

$$\begin{cases} Q = \displaystyle\sum_{R_d=R_b}^{R_d=L_R} \Delta q(R_d) = 2nR_b^{n-1}\displaystyle\int_{R_b}^{L_R} \dfrac{R_d^n T(R_d)dR_d}{XR_d^{2n} + YR_b^{2n}} \\ \quad = 2nR_b^{n-1}g(R_b) \\ g(R) = \displaystyle\int_R^{L_R} \dfrac{R_d^n T(R_d)dR_d}{XR_d^{2n} + YR_b^{2n}} \qquad (R \le R_d \le L_R) \end{cases} \tag{16}$$

When $R_d = L_R$, the radial displacement and stress at R can be rewritten as follows:

$$\begin{cases} u(L_R, R) = \left[Y(X - N)(\dfrac{R_b}{R}) - Y(Y + X)(\dfrac{R}{R_b})\right]\dfrac{R_b^n}{E_\theta}g(R) \\ \sigma_r(L_R, R) = -\left[Y(\dfrac{R_b}{R}) - X(\dfrac{R}{R_b})^{n-1}\right]R_b^{n-1}g(R) \\ \sigma_\theta(L_R, R) = T(R) + \left[Y(\dfrac{R_b}{R}) - X(\dfrac{R}{R_b})^{n-1}\right]nR_b^{n-1}g(R) \end{cases} \tag{17}$$

The radial displacement and stress of the core mould can be expressed as follows.

$$\begin{cases} u^m(L_R, R) = -\dfrac{2nR_b^{n+1}g(R_b)}{E^m(R_b - R_c)} \\ \qquad \left[(1 - u^m)R + (1 + u^m)\right]\dfrac{R_c}{R} \\ \sigma_r^m(L_R, R) = -\dfrac{2nR_b^{n+1}g(R_b)}{(R_b - R_c)}(1 - \dfrac{R_c^2}{R^2}) \\ \sigma_\theta^m(L_R, R) = -\dfrac{2nR_b^{n+1}g(R_b)}{(R_b - R_c)}(1 + \dfrac{R_c^2}{R^2}) \end{cases} \tag{18}$$

The tension of whole thick-walled is $T(L_R)$ as shown in (19).

$$\sigma_r(L_R, R) = -q(R) = -\dfrac{L_R - R}{R}\sigma_\theta(L_R, R) = -\dfrac{L_R - R}{R}T(L_R) \tag{19}$$

Substitute (19) into (17), then

$$g(R) = \dfrac{L_R - R}{R}\dfrac{T(L_R)}{\left[Y(\frac{R_b}{R})^{n+1} + X(\frac{R}{R_b})^{n-1}\right]R_b^{n-1}} \tag{20}$$

According to (21), the required tension of each layer can be calculated.

$$T(R) = \left[1 + n(\dfrac{L_R - R}{R})(\dfrac{\frac{X}{Y}(\frac{R}{R_b})^{2n} - 1}{\frac{X}{Y}(\frac{R}{R_b})^{2n} + 1})\right]T(L_R) \tag{21}$$

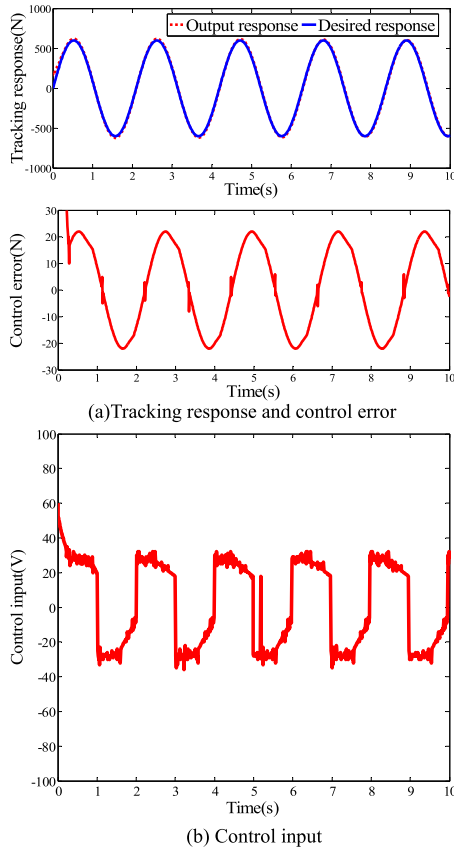**FIGURE 11.** Sin response of PID (simulation).

FIGURE 12. Step response of SMC with sgn(s) (simulation).

III. NONLINEAR DYNAMICS MODEL OF TENSION CONTROL SYSTEM

The tension control process is shown in **Fig.2**, and the tension is controlled by detecting and controlling the torque of the torque motor. Because of the complexity of fiber tape winding motion and the time-varying of tension exerted, tension control system needs good dynamic performance. The speed of the fiber tape is determined by the rotation speed of winding machine spindle and the radius of the winding products. Due to the constant speed of the core mould, the linear velocity of the fiber tape is difficult to remain constant and the change law of linear velocity is very complicated.

Consider the effect of velocity on tension, dynamic analysis of the tension control system is carried out, and the moment equation of dynamic equilibrium is established as follows:

$$M(t) = T_0(t)R_T + \frac{J_T}{R_T} \times \frac{dv(t)}{dt} \qquad (22)$$

$$T_R(t) - T_0(t) = \frac{J_T}{R_T^2} \times \frac{dv(t)}{dt} + f_x \qquad (23)$$

where, $M(t)$, J_T, T_0, T_R, are motor torque, the rotational inertia of the motor, tension produced by torque motor and tension acting on the winding layer, respectively, f_x is total friction of mechanical structure, v is velocity of fiber tape, and R_T is radius of torque motor.
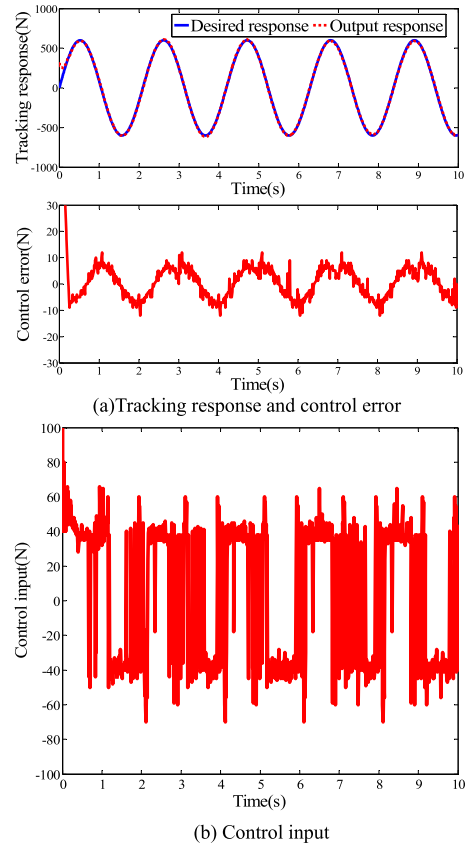
According to **Fig.3**, mathematical model of torque motor can be established as follows [36], [37]:

$$\begin{cases} M(t) = \dfrac{K\left[U_a(t) - \omega K_1 - L\dfrac{dI_a(t)}{dt}\right]}{R_a} \\ \begin{cases} M(t) = KI_a(t) \\ \varepsilon_1 = -\omega K_1 \\ \varepsilon_2 = -L\dfrac{dI_a(t)}{dt} \\ I_a(t) = \dfrac{[U_a(t) + (\varepsilon_2 + \varepsilon_1)]}{R_a} \end{cases} \end{cases} \qquad (24)$$

where, R_a, I_a, ε_1, ε_2, are Armature resistance, armature inductance, back electromotive force of motor and induced electromotive force of motor, respectively, U_a is input voltage, K_1 is back EMF constant, and K is torque sensitivity. According to the characteristics of torque motor, the output torque is highly linear and directly proportional to the armature current.

Essentially, tension control system is a nonlinear deadzone system resulted from external interference and friction. Assuming $v = x_1$, then the nonlinear differential equation with dead-zone characteristic can be rewritten as follows:

$$\begin{cases} \dot{x}_1 = x_2 \\ \dot{x}_2 = f(\pmb{x}, t) + d(t) + B(t)w(u) = a(t) \end{cases} \qquad (25)$$

where, $\pmb{x} = [x_1, x_2]^T \in \mathbf{R}^2, f(\pmb{x}, t) \in \mathbf{R}, B(t) \in \mathbf{R}, \mu(t) \in \mathbf{R}$ are state vector, unknown nonlinear function, control gain and
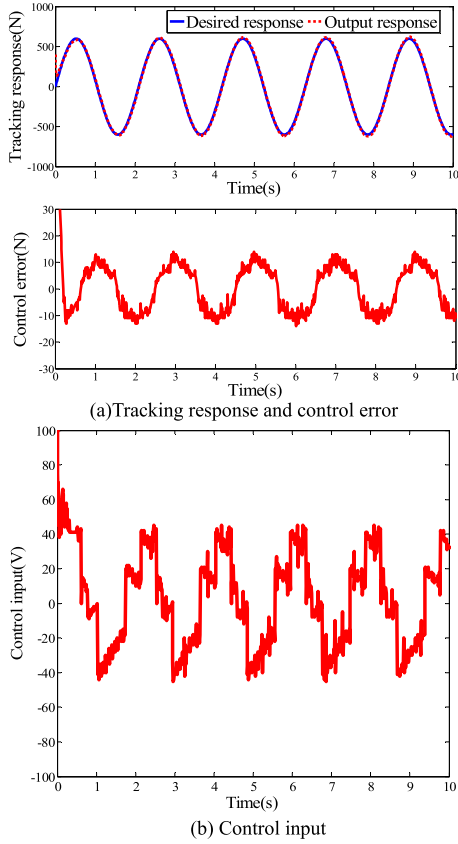
FIGURE 13. Step response of SMC with sat(s) ($\delta = 0.02$) (simulation).
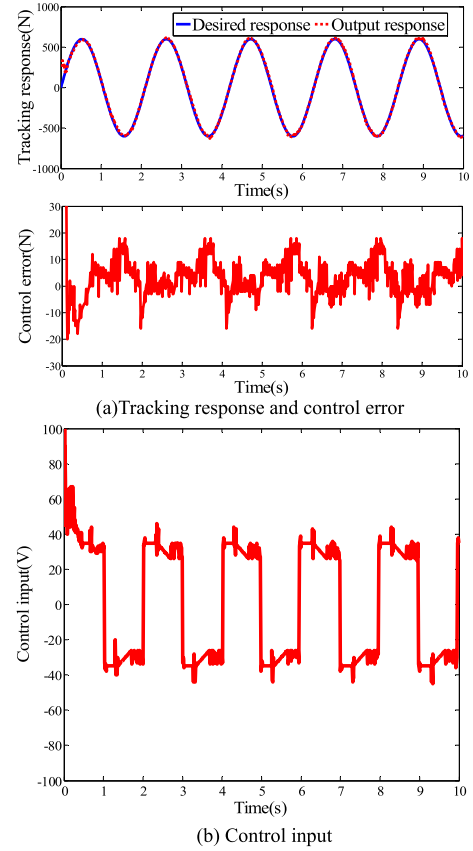

FIGURE 14. Step response of SMC with sat(s) ($\delta = 0.05$) (simulation).

control input, respectively, $|d(t)| < \rho(\rho > 0)$ is the external disturbance, $a(t)$ is continuously differ-entiable, and $a(t)$ is continuously differentiable.

According to **Fig.4**, $w(u) \in \mathbf{R}$ is the nonlinear function of dead-zone which can be expressed as follows [38]:

$$w(u) = \begin{cases} m_r(u - b_r), & u > b_r \\ 0, & b_l \le u \le b_r \\ m_l(u - b_l), & u < b_l \end{cases} \quad (26)$$

where m_r and m_l are slopes of the dead-zone function, b_r, b_l are thresholds of the dead-zone.

IV. ESO-BASED ASMC
A. DESIGN OF THE ESO
The control block diagram of ESO-based ASMC is shown in **Fig.5**. By adding a state variable x_3 , (25) can be expre-ssed as follows:

$$\begin{cases} \dot{x}_1 = x_2 \\ \dot{x}_2 = x_3 = a(t) \\ \dot{x}_3 = \dot{a}(t) \end{cases} \quad (27)$$

Structure of the ESO with observation states $\hat{x}_i(i = 1, 2, 3)$ can be rewritten as follows [39]–[41]:

$$\begin{cases} \dot{x}_1 = \hat{x}_2 - k_1(\hat{x}_1 - x_1) \\ \dot{x}_2 = \hat{x}_3 - k_2(\hat{x}_1 - x_1) \\ \dot{x}_3 = -k_3(\hat{x}_1 - x_1) \end{cases} \quad (28)$$

where k_i is the constant.

Define the state errors as $\Delta x_i = \hat{x}_i, x_i$, and (29) can be obtained by (28) minus (27).

$$\begin{cases} \Delta \dot{x} = A \Delta x + e \\ \begin{cases} \Delta \dot{x} = \begin{bmatrix} \Delta x_1 & \Delta x_2 & \Delta x_3 \end{bmatrix}^T \\ A = \begin{bmatrix} -k_1 & 1 & 0 \\ -k_2 & 0 & 1 \\ -k_3 & 0 & 0 \end{bmatrix} \\ e = \begin{bmatrix} 0 & 0 & -\dot{a}(t) \end{bmatrix}^T \end{cases} \end{cases} \quad (29)$$

The characteristic equation of matrix A can be expressed as follows:

$$s^3 + k_1 s^2 + k_2 s + k_3 = 0 \quad (30)$$

By selecting the appropriate k_i based on the pole assign-ment method, the observed state variables are guaranteed to asymptotic tracking the actual values. The dynamic behave-ior of closed-loop system is mainly determined by poles.
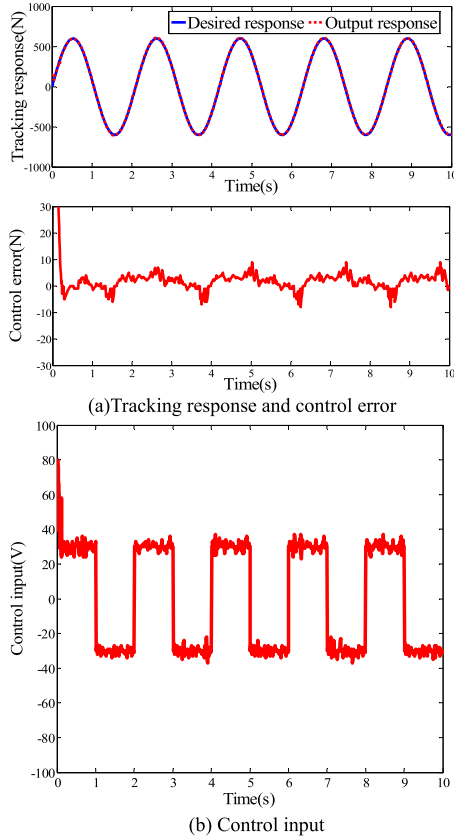
FIGURE 15. Sin response of ASMC (simulation).

FIGURE 16. Step response of traditional PID (experiment).

The parameter matrix determined by trial and error method has a certain blindness. Based on the state variable feedback controller, hyperplane parameter design based on pole assignment is proposed. Pole assignment is to change the pole distribution through the selection of feedback matrix so that the system tends to be stable.

B. DESIG OF THE ASMC

$$
\begin{cases}
\boldsymbol{x}_{\mathrm{d}} = [x_{\mathrm{d}}, 0]^T \\
\boldsymbol{e} = \boldsymbol{x} - \boldsymbol{x}_{\mathrm{d}} = [x_1, x_2]^T - [x_{\mathrm{d}}, 0]^T = [e_1, e_2]^T
\end{cases}
\tag{31}
$$

where $\boldsymbol{x}_{\mathrm{d}} = 0$ is signal, and $\boldsymbol{e}$ is system control error.

Select the following sliding mode surface:

$$
s = e_2 + c_1 e_1 = x_2 + c_1(x_1 - x_{\mathrm{d}})
\tag{32}
$$

The following can be obtained from (25):

$$
\dot{x}_2 = f + d + Bw = f + d + (B_0 + \Delta B)w = f + d_1 + B_0 w
\tag{33}
$$

where B_0 is the control gain, ΔB is the variation of control gain, (ΔB) is the disturbance.

According to (29), (32) can be rewritten as follows:

$$
\begin{aligned}
s &= (\hat{x} - \Delta x_2) + c_1 (\hat{x}_1 - \Delta x_1 - x_{\mathrm{d}}) \\
&= \hat{x}_2 + c_1(\hat{x}_1 - x_{\mathrm{d}}) - \Delta x_2 - c_1 \Delta x_1 \\
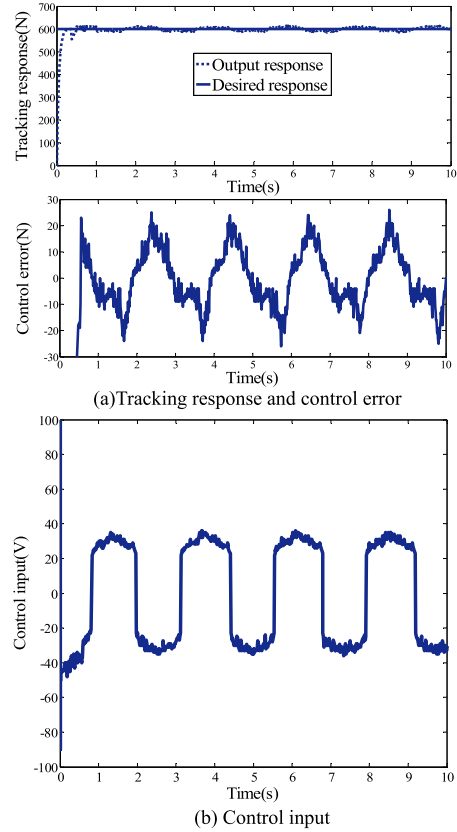&= \hat{s} - \Delta x_2 - c_1 \Delta x_1
\end{aligned}
\tag{34}
$$

where

$$
\dot{\hat{s}} = \dot{\hat{x}}_2 + c_1 \dot{\hat{x}}_1 = \Delta \dot{x}_2 + \dot{x}_2 + c_1 \dot{\hat{x}} = \Delta \dot{x}_2 + f + d_1 + B_0 + c_1 \dot{\hat{x}}_1.
\tag{35}
$$

Assuming $\dot{\hat{s}} = 0$, $\Delta \dot{x}_2 = 0$, then the equivalent control can be expressed as follows.

$$
w_{\mathrm{eq}} = B_0^{-1}(-f - d_1 - c_1 \dot{\hat{x}}_1)
\tag{36}
$$

The switching control can be written as follows:

$$
w_{\mathrm{sw}} = -k_{\mathrm{d}}\hat{s} - k\,sat(\hat{s}/\varepsilon)
\tag{37}
$$

where, $\varepsilon > 0$, $\eta_2 \leq k_{\mathrm{d}}\varepsilon + k$, and $\eta_2 > 0$.

And the system control input can be expressed as follows:

$$
w_{\mathrm{d}} = w_{\mathrm{eq}} + w_{\mathrm{sw}}
\tag{38}
$$

where, $w_{\mathrm{d}} \approx w$, and w is the actual control input.

Suppose

$$
\dot{\hat{w}}_{\mathrm{d}} = -\delta \hat{w}_{\mathrm{d}} + \delta w_{\mathrm{d}}
\tag{39}
$$

where $\delta > 0$ and $\lim\limits_{t \to \infty} \hat{w}_{\mathrm{d}} = w$.

According to (29) and (33), (38) can be rewritten as follows:

$$
w_{\mathrm{d}} = B_0^{-1}(-\dot{\hat{x}}_2 + B_0 \hat{w}_{\mathrm{d}} - c_1 \dot{\hat{x}}) - k_{\mathrm{d}}\hat{s} - k\,sat(\hat{s}/\varepsilon)
\tag{40}
$$
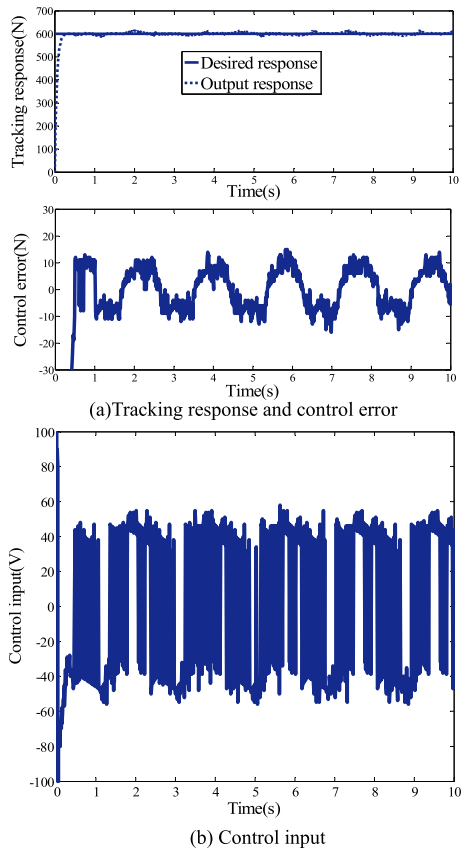
FIGURE 17. Step response of SMC with sgn(s) (experiment).

FIGURE 18. Step response of SMC with sat(s) ($\delta = 0.02$) (experiment).

C. DEAD-ZONE COMPENSATION

Suppose the compensation input of dead-zone is as follows [42]:

$$u = \begin{cases} m_r^{-1}(w_d + \hat{m}_r\hat{b}_r), & e_1 < -e_d \\ 0, & |e_1| \leq e_d \\ \hat{m}_l^{-1}(w_d + \hat{m}_l\hat{b}_l), & e_1 > e_d \end{cases} \quad (41)$$

where e_d is the desired steady state error.

Define $N[n_r, n_1], \boldsymbol{M} = [m_r, m_1]^T, \boldsymbol{\theta} = [m_r b_r, m_l b_l]^T$, and

$$n_r \begin{cases} 1, & (e_1 < e_d) \\ 0, & (e_1 \geq -e_d) \end{cases} \quad n_l \begin{cases} 1, & (e_1 < e_d) \\ 0, & (e_1 \geq -e_d) \end{cases}$$

Define $\phi = [m_r/m_r, m_l/m_l]^T = [1, 1]^T$, and its estimated value is $\hat{\phi}[m_r/\hat{m}_r, m_l/\hat{m}_l]^T$, where estimation errors of $\boldsymbol{\theta}$ and ϕ are $\tilde{\boldsymbol{\theta}} = \hat{\boldsymbol{\theta}} - \boldsymbol{\theta}$ and $\tilde{\phi} = \hat{\phi} - \phi$, respectively, $\hat{\boldsymbol{\theta}}$ and $\hat{\phi}$ can be obtained from the following adaptive law:

$$\begin{cases} \dot{\hat{\boldsymbol{\theta}}} = \dot{\tilde{\boldsymbol{\theta}}} = -aN^T s_\varepsilon \\ \dot{\hat{\phi}} = \dot{\tilde{\phi}} = -\beta N^T H s_\varepsilon \\ H = w_d + N\hat{\boldsymbol{\theta}} \\ s_\varepsilon = \hat{s} - \varepsilon \cdot sat(\hat{s}/\varepsilon) \end{cases} \quad (42)$$

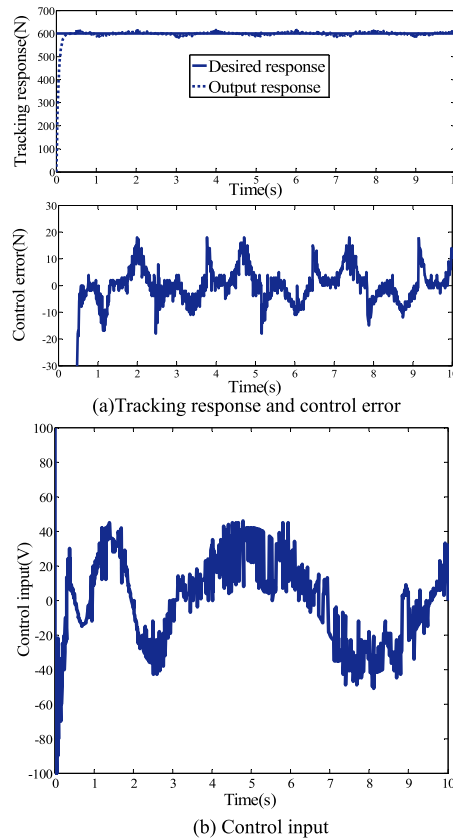where α and β are change rates of the adaptation.

According to $|\hat{S}| \leq \varepsilon, S_\varepsilon$, and (41) can be rewritten as follows:

$$u = \left(N\hat{\boldsymbol{M}}\right)^{-1}\left(w_d + N\hat{\boldsymbol{\theta}}\right) \quad (43)$$

where $\hat{\boldsymbol{M}}$ can be obtained from the adaptation of

$$\hat{m}_j(j = r, l).$$
$$\hat{m}_{j,n+1} = \hat{\phi}_{j,n}\hat{m}_{j,n} \quad (44)$$

where n is the number of updates.

According to (43), then

$$w = NMu - N\boldsymbol{\theta} = (NM)(N\hat{\boldsymbol{M}})^{-1}(w_d + N\hat{\boldsymbol{\theta}}) - N\boldsymbol{\theta} \quad (45)$$

Substitute (45) into (35), then

$$\begin{aligned}
\dot{\hat{s}} &= \Delta\dot{x}_2 + f + d_1 + B_0 \begin{bmatrix} (NM)(N\hat{\boldsymbol{M}})^{-1} \\ (w_d + N\hat{\boldsymbol{\theta}}) \\ -N\boldsymbol{\theta} \end{bmatrix} + c_1\dot{x}_1 \\
&= \Delta\dot{x}_2 + f + d_1 + B_0 \\
&\quad \times \begin{bmatrix} \left(1 + N\tilde{\phi}\right) \begin{pmatrix} B_0^{-1}(-\dot{\hat{x}}_2 + \\ B_0\hat{w}_d - c_1\dot{\hat{x}}) \\ -k_d\hat{s} \\ -ksat(\hat{s}/\varepsilon) \\ +N\hat{\boldsymbol{\theta}} \end{pmatrix} - N\boldsymbol{\theta} \end{bmatrix} + c_1\dot{x}_1 \\
&= \Delta\dot{x}_2 + f + d_1 - \dot{\hat{x}}_2 + B_0\hat{w}_d - c_1\dot{\hat{x}} - B_0k_d\hat{s} \\
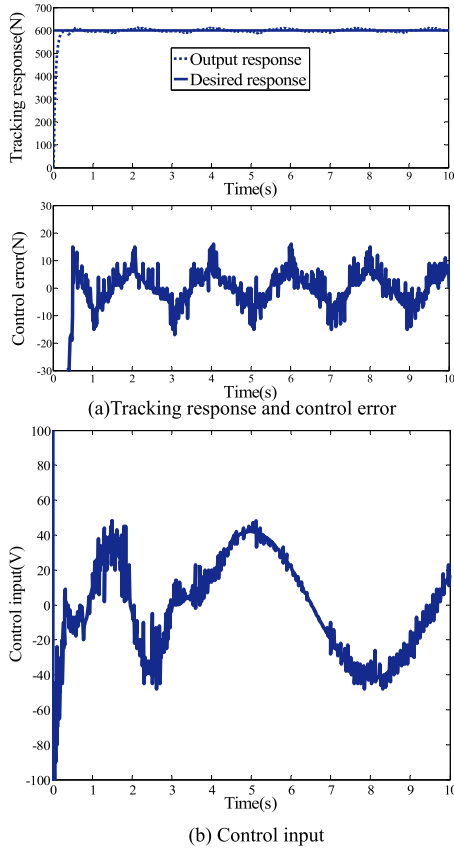&\quad - B_0ksat(\hat{s}/\varepsilon)
\end{aligned}$$

FIGURE 19. Step response of SMC with sat(s) ($\delta = 0.05$) (experiment).

FIGURE 20. Step response of ASMC (experiment).

$$+B_0 N\hat{\boldsymbol{\theta}} - B_0 N\boldsymbol{\theta} + c_1\dot{\tilde{x}}_1 + B_0 N\tilde{\phi}\left(w_d + N\hat{\boldsymbol{\theta}}\right)$$
$$= \Delta\dot{x}_2 + f + d_1 - \dot{\hat{x}}_2 + B_0\hat{w}_d - c_1\dot{\hat{x}} - B_0 k_d\hat{s}$$
$$\quad -B_0 k sat(\hat{s}/\varepsilon)$$
$$\quad +B_0 N\hat{\boldsymbol{\theta}} + B_0 N\tilde{\phi}H$$
$$= B_0\left[\hat{w}_d - w - k_d\hat{s} - k sat(\hat{s}/\varepsilon) + N\hat{\boldsymbol{\theta}} + N\tilde{\phi}H\right] \quad (46)$$

The state variables of the system can asymptotically track the desired signals by the action of the sliding surface $\hat{s}$ and the control law, which can be proved by Lyapunov function.

$$V = \frac{1}{2}\left[\frac{1}{B_0}s_\varepsilon^2 + \frac{1}{a}\tilde{\theta}^T\tilde{\theta} + \frac{1}{\beta}\tilde{\phi}^T\tilde{\phi}\right] \quad (47)$$

$$\dot{V} = \frac{1}{B_0}s_\varepsilon\dot{\hat{s}} + \frac{1}{a}\dot{\tilde{\theta}}^T\tilde{\theta} + \frac{1}{\beta}\dot{\tilde{\phi}}^T\tilde{\phi} \quad (48)$$

When $|\hat{s}| < \varepsilon$, $s_\varepsilon = 0$, $\dot{V} = 0$ can be obtained from (42).

Next, we should prove that $\dot{V} \leq 0$ is founded, when $|\hat{s}| \geq \varepsilon$. Substitute (46) into (48), then

$$\dot{V} = \left[\hat{w}_d - w - k_d\hat{s} - k sat(\hat{s}/\varepsilon) + N\hat{\boldsymbol{\theta}} + N\tilde{\phi}H\right]$$
$$\quad + \frac{1}{a}\dot{\tilde{\theta}}^T\tilde{\theta} + \frac{1}{\beta}\dot{\tilde{\phi}}^T\tilde{\phi} \quad (49)$$

Substitute (42) into (49), then

$$\dot{V} = \left[\hat{w}_d - w - k_d\hat{s} - k sat(\hat{s}/\varepsilon)\right]$$
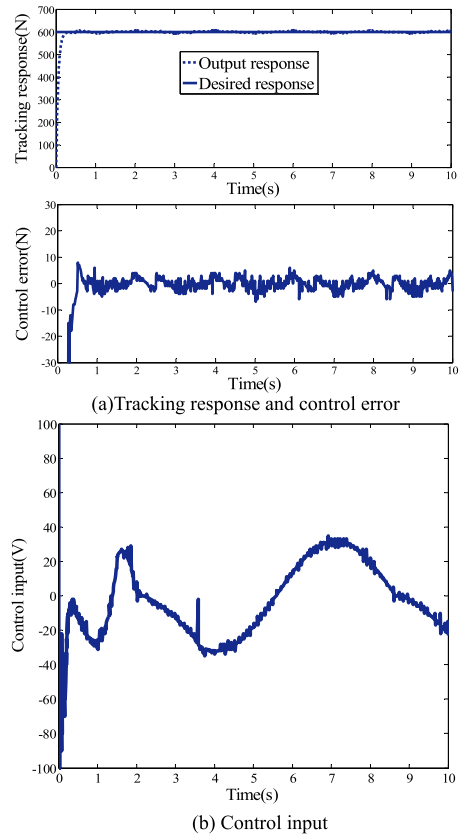$$\quad \leq \eta_2|s_\varepsilon| - k_d\hat{s}^2 - k_d\varepsilon|s_\varepsilon| - k|s_\varepsilon| \quad (50)$$

By selecting the sufficiently large parameters k_d and k, $\eta^2 \leq k_d\varepsilon + k$ can be founded. Thus

$$\dot{V} \leq -k_d s_\varepsilon^2 \leq 0 \quad (51)$$

Subsequently, when $t \to \infty$, $s_\varepsilon(t) \to 0$. Due to $s_\varepsilon = \hat{s} - \varepsilon.sat(\hat{s}/\varepsilon)$, and $\hat{s} = \hat{x}_2 + c_1(\hat{x}_1 - \hat{x}_d)$, $|\hat{s}| < \varepsilon$ and $\hat{x}$ is bounded. According to the principle of ESO, $\hat{x} \to \hat{x}_2$ and x_1 can asymptotically track the desired signal x_d.

V. SIMULATION ANALYSES AND EXPERIMENTAL VERIFICATIONS

A. SIMULATION ANALYSES

The mathematical model of tension control system is used as the controlled object to verify the designed control algorithm. A step signal ($r_1(t) = 600N$) is used for positioning control and a sinusoidal signal ($r_2(t) = 600sin(\pi t)N$) is used for tracking control.

An Advantech PCI-728 2-way isolated analog output card, PCL-730 digital input and output card, PCI-1680U data acquisition card are used for data output, conversion and acquisition. As shown in **Fig.27**, the experiment is carried out on XP-1 large-scale numerical control composite fabric tape winding machine.

The simulation results of sine response and step response are shown in **Figs. 6-15**. **Figs. 6** and **11** are the simulation results of the PID algorithm, the average control error of the sinusoidal response and step response is 18.963N, which
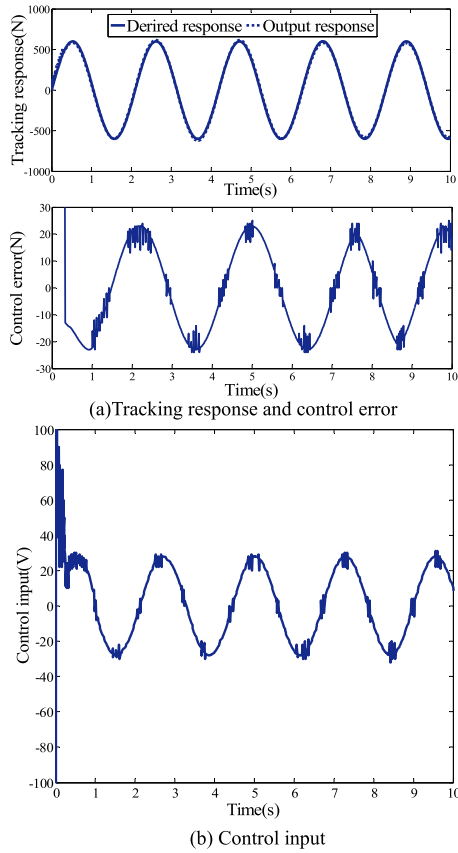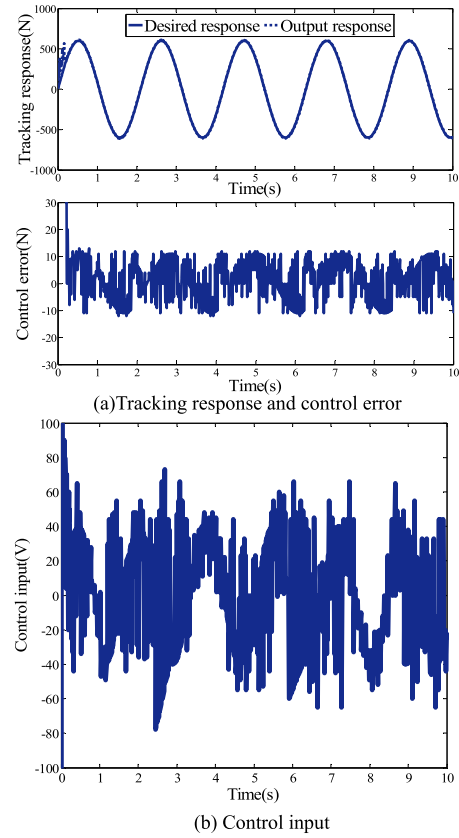
FIGURE 21. Sin response of PID (experiment).

FIGURE 22. Sin response of SMC with sgn(s) (experiment).

is the largest error compared to other controllers. **Figs. 7** and **12** show that the average control error of sgn algorithm is 8.199N. Compared with PID algorithm, sgn algorithm can reduce control error effectively. However, from the perspective of control input, the sgn algorithm generates high-frequency chattering, which affects the dynamic characteristics of the system and motor safety. In order to reduce the control input chattering, a SMC with sat(s) control algorithm is proposed. The simulation results of sat(0.02) in **Fig. 8** and **13** show that the average control error is 9.923N, which effectively reduces chattering and increases the control error. Compared with sgn, sat(0.02) reduces chattering at the cost of sacrificing control error. The simulation results of sat(0.05) in **Figs. 9** and **14** show that the average control error is 11.912N. Compared with the simulation results of sat(0.02), the control error is larger and the chattering is smaller. For the sat(s) control algorithm, the simulation results show that the thicker the boundary layer, the larger the control error and the smaller the control input chattering. **Figs. 10** and **15** show that the average control error is 4.056N. Compared PID, sgn, sat(0.02) and sat(0.05), control error of the design ESO-based ASMC is reduced by 78.6%, 50.5%, 59.1% and 65.9%, respectively.

B. EXPERIMENTAL VERIFICATIONS

The experiment uses C++ to write control program and IPC-620-L as controller carrier. The designed algorithm

TABLE 1. Performance comparison of different control algorithms (simulation).

	Response	PID	SMC			ASMC
			sgn(s)	sat(φ=0.02)	sat(φ=0.05)	
Control error(N)	Step	18.584	7.836	9.420	11.342	4.248
	Sin	19.322	8.563	10.426	12.482	3.864
Chattering extent			Smaller	Larger	Large	Moderate	Small

TABLE 2. Performance comparison of different control algorithms (experiment).

	Response	PID	SMC			ASMC
			sgn(s)	sat(φ=0.02)	sat(φ=0.05)	
Control error(N)	Step	20.342	9.578	10.834	12.226	5.262
	Sin	21.082	10.24	13.248	17.784	4.247
Chattering extent			Smaller	Larger	Large	Moderate	Small

control programs include analog and digital signal conversion, measuring function of pressure sensor and sampling.

The experimental results are shown in **Figs.16-25**, **Figs.16** and **21** show that the average control error of PID experimental results is 20.712N, **Figs.17** and **22** show that the average control error of sgn experimental results is 9.909N, **Figs.18** and **23** show that the average control error of sat(0.02) experimental results is 12.041N, **Figs.19** and **24** show that

FIGURE 23. Sin response of SMC with sat(s) ($\delta = 0.02$) (experiment).
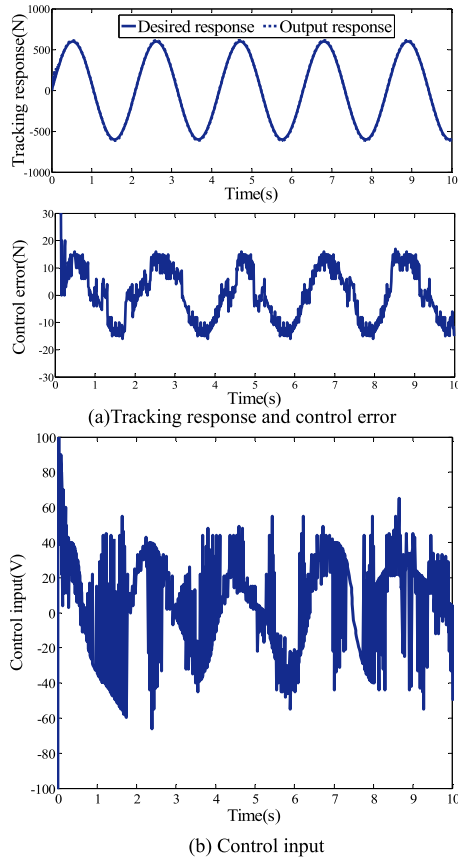

FIGURE 24. Sin response of SMC with sat(s) ($\delta = 0.05$) (experiment).

the average control error of sat(0.05) experi-mental results is 15.005N, and **Figs.20** and **25** show that the average control error of ASMC experimental results is 4.755N. The comparison between the experimental results and the simulation results shows the same trend. By comparing the data in **Tables.1-2** and analyzing the control error changes in **Fig.26**, it can be shown that ASMC has obvious advantages over the other four control algorithms. Compared with PID, SMC with sat ($\varphi = 0.05$), SMC with sat ($\varphi = 0.02$) and SMC with sgn, the designed ASMC algorithm reduces the average control errors of sinusoidal response and step response by 78%, 51%, 60% and 67%, respectively.

In order to further verify the feasibility and validity of the ASMC algorithm. Different tension control strategies are used in winding experiments, and the changes of void content and residual stress are observed. Two different composite prepreg tapes are applied to the experiment, the relevant parameters of the prepreg is shown in **Table 3**. During the winding process, the key process parameters that affect the product performance are fabric tension, cylinder thrust, hot air temperature and winding speed, which are set as 600N, 1000N, 80°C and 16m/min, respectively. The curing process has a great influence on the properties of the products. In this experiment, the ambient temperature is (20±2)°C, the curing pressure is 0.2Mpa, the relative humidity is (25±2)%, and the heating rate is 3°C/min. rate is 3°C/min.

Voids in composite prepreg tape winding products are defects that principally exist between tape layers due to residual air bubbles, resin flow, and sufficient compaction during resin flow. Therefore, void content have a signify-cant influence on the mechanical performance of composite material products. Density measurements, microscopy **[43]**–**[50]**, ultrasonic attenuation **[51]**, and X-ray computed tomo-graphy **[52]** can be used to measure void content. The electron microphotography method specified in GB/T3365-2008 **[53]** provides the highest porosity detection accuracy. The fraction of the total pore area was measured with an optical microscope. The specimen was sampled and observ-ed at the marked position, as shown in **Fig.28**. The samples are cut on the composite ring product, with length, width and height of 20mm, 10mm and 10mm, respectively. The samples are ground and polished under flowing water, then the polished specimen is observed under a microscope, and the process of measuring void content is shown in **Fig.29**.

Void content can be calculated using the following equation.

$$S_{\mathrm{x}} = \frac{S_v}{S_t} \times 100\% \tag{52}$$

where S_{x} is the void content, S_{v} is the total void area, and S_{t} is the cross-sectional area of the specimen.

(a)Tracking response and control error

(b) Control input
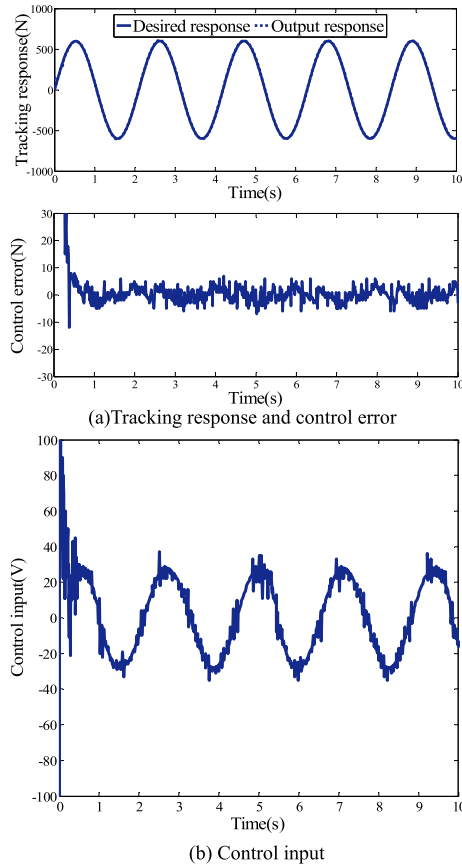
FIGURE 25. Sin response of ASMC (experiment).

(a) Step response

(b) Sin response

FIGURE 26. Control errors comparison.

High precision on-line rectify deviation controller
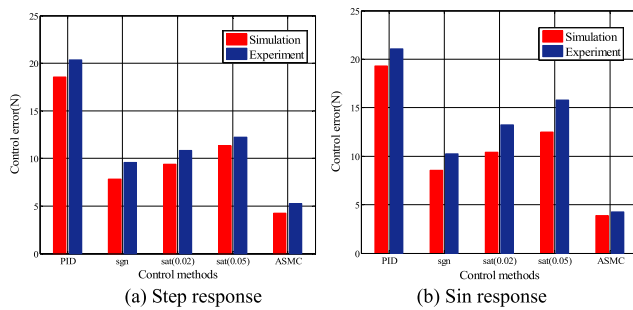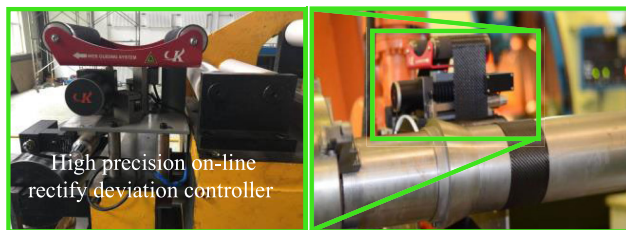
FIGURE 27. Composite prepreg tape winding experiment.

Residual stress is inevitable during composite prepreg winding due to deformation of the products. Excessive residual stress has a great influence on the structural
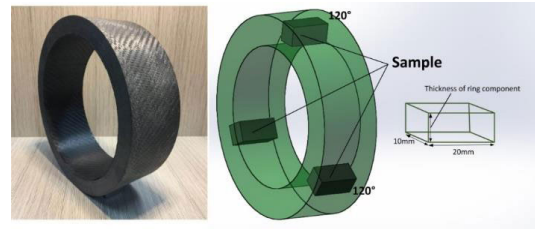

FIGURE 28. Photograph and sketch of the samples for testing void content.

TABLE 3. The relevant parameters of the prepreg.

Materials	Type	Tape thickness	Braiding angle	Fiber volume fraction	Tape width
High silica glass fiber /phenolic resin	BWT26082 /DFQS-3	0.22mm	(0°) unidirectional	(48±2)%	80mm
Carbon fiber /epoxy resin	T-300/ YH-69	0.25mm	(0°/90°) orthogonal	(56±2)%	80mm

performance, thus the residual stress is the key index to evaluate the performance of the product. Therefore, the residual stress is chosen as one of the optimization objectives. The slitting method is widely used to calculate residual stress in composite structures. When examining residual stress in composite annular parts, a slot is cut along the radial direction, and the slot position will change due to the residual stress moment. **Fig.30** shows the change in slot displacement after closure of the compound ring, which can be measured with an electron microscope. The circumfere-ntial residual stress in the composite ring can be calculated with the following equations [54], [55].

$$
\sigma_\lambda = -\frac{4M_r}{k_\lambda}
$$
$$
\times \left(\frac{-R_x^2 R_y^2}{r^2} \ln \frac{R_x}{R_y} + R_y^2 \ln \frac{r}{R_y} + R_x^2 \ln \frac{R_y}{r} + R_y^2 - R_x^2 \right)
$$
(53)

$$
\begin{cases}
M_r = -\frac{\Delta E}{8\pi} \left(\frac{\left(R_y^2 - R_x^2\right)^2 - 4R_x^2 R_y^2 \left[\ln\left(R_y/R_x\right)\right]^2}{2\left(R_y^2 - R_x^2\right)} \right) \\
k_\lambda = \left(R_y^2 - R_x^2\right)^2 - 4R_x^2 R_y^2 \left[\ln\left(R_y/R_x\right)\right]^2 \\
\tau = \tau_1 + \tau_2
\end{cases}
$$
(54)

where R_x and R_y are the inner and outer radii, respectively, r is the current position and τ is the total displacement of the slot.

The formula for calculating the residual stress of the composite ring specimen can be defined as follows:

$$
\sigma_\tau = \frac{|\sigma_\lambda\left(r = R_x\right)| + |\sigma_\lambda\left(r = R_y\right)|}{2}
$$
(55)

Winding experimental results of different algorithms are summarized in **Tables 4**, and variation of the void
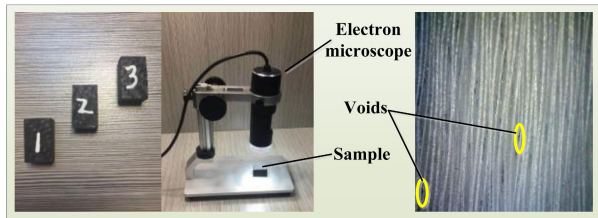
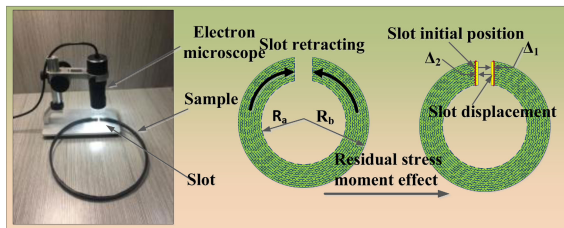**FIGURE 29.** Process for measuring void content of composite tape winding products.

FIGURE 30. Slitting method for measuring residual stress.

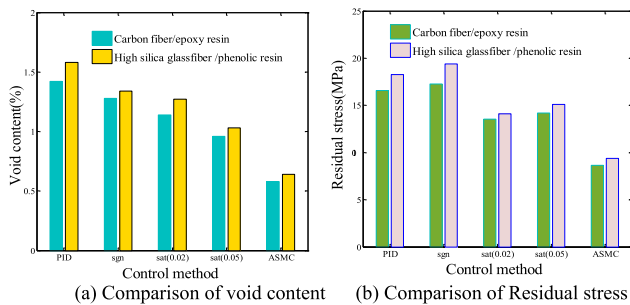(a) Comparison of void content (b) Comparison of Residual stress

FIGURE 31. Comparison of properties of composite tape winding products.

TABLE 4. Comparison of properties of composite tape winding products.

Parameter	Type	PID	SMC			ASMC
			sgn(s)	sat(φ=0.02)	sat(φ=0.05)	
Void content (%)	T-300/ YH-69	1.42	1.28	1.14	0.96	0.58
	BWT26082 /DFQS-3	1.58	1.34	1.27	1.03	0.64
Residual stress (MPa)	T-300/ YH-69	16.58	17.26	13.56	14.20	8.64
	BWT26082 /DFQS-3	18.28	19.37	14.10	15.12	9.36

content and residual stress are illustrated in **Fig. 31**. Experiment with T-300/YH-69, it can be known that the designed ASMC has reduced the void content by about 58%, 39%, 49% and 54% and reduced the residual stress by about 48%, 39%, 36% and 50% when compared with the PID, SMC with sat(s) (φ = 0.05), SMC with sat(s) (φ = 0.02) and SMC with sgn(s). Experiment with BWT26082/DFQS-3, it can be known that the designed ASMC has reduced the void content by about 59.4%, 37.9%, 49.6% and 52.2% and reduced the residual stress by about 48.8%, 38.1%, 33.6% and 51.6% when compared with

the PID, SMC with sat(s) (φ = 0.05), SMC with sat(s) (φ = 0.02) and SMC with sgn(s). Experimental results show that ASMC algorithm can reduce the void content and residual stress of winding products. The decrease of void content and residual stress of winding products reflects the improvement of control accuracy of tension system.

VI. CONCLUSIONS

In this paper, the mechanical analysis of the composite products micro-body is carried out, and the tension calculation model is established. According to the tension calculation model, it can be known that the application of tension value is time-varying in the winding process. Compared with the traditional constant tension winding, variable tension processing can better guarantee the mechanical properties of composite products. Therefore, higher requirements are required for the control accuracy and sensitivity of the tension system controller.

The mathematical model of tension control system is established. The tension control system is complex, susceptible to uncertain interference and nonlinear dead-zone. In order to ensure high control accuracy of tension control system, a robust control algorithm ESO-based ASMC is proposed. In the case of system model parameter uncertainty and load disturbance. By using the extended state observer to estimate and compensate the total disturbance, the influence of the total disturbance on the control accuracy can be reduced and the dynamic performance of the system can be improved. The upper bound of system observation error cannot be obtained accurately. The parameter adaptive law is adopted to adjust the switching control gain, which effectively reduces the chattering of the system and ensures the tracking accuracy of the system output. Finally, Lyapunov theory is used to verify the stability of the closed-loop system.

Simulation and experimental results show that the designed ASMC has highest control precision and stronger interference suppression, smaller steady-state error, and robustness when compared with other four controllers. ASMC can also effectively improve the machining quality, stability, consistency, and other properties of composites winding product. In addition, the adaptive controller can also be widely used in industrial robot manufacturing systems, such as grinding, welding and spraying.

REFERENCES

[1] H. Li, Z. Wang, J. Y.-L. Forrest, and W. Jiang, "Low-velocity impact localization on composites under sensor damage by interpolation reference database and fuzzy evidence theory," *IEEE Access*, vol. 6, pp. 31157–31168, 2018.

[2] Y. Chen, J. Zhang, and Y. Gong, "Utilizing anisotropic fabrics composites for high-strength soft manipulator integrating soft gripper," *IEEE Access*, vol. 7, pp. 127416–127426, 2019.

[3] M. Jalali, T. Molière, A. Michaud, and R. Wuthrich, "Multidisciplinary characterization of new shield with metallic nanoparticles for composite aircrafts," *Compos. B, Eng.*, vol. 50, pp. 309–317, Jul. 2013.

[4] D. Kim, T. Centea, and S. R. Nutt, "Out-time effects on cure kinetics and viscosity for an out-of-autoclave (OOA) prepreg: Modelling and monitoring," *Compos. Sci. Technol.*, vol. 100, pp. 63–69, Aug. 2014.

[5] T. Centea, L. K. Grunenfelder, and S. R. Nutt, "A review of out-of-autoclave prepregs–material properties, process phenomena, and manufacturing considerations," *Compos. A, Appl. Sci. Manuf.*, vol. 70, pp. 132–154, Mar. 2015.

[6] B. Deng and Y. Shi, "Modeling and optimizing the composite prepreg tape winding process based on grey relational analysis coupled with BP neural network and bat algorithm," *Nanosc. Res. Lett.*, vol. 14, no. 1, Aug. 2019.

[7] C. Kang, Y. Shi, X. He, T. Yu, B. Deng, H. Zhang, P. Sun, and W. Zhang, "Multi-response optimization of T300/epoxy prepreg tape-wound cylinder by grey relational analysis coupled with the response surface method," *Mater. Res. Exp.*, vol. 4, no. 9, Sep. 2017, Art. no. 095301.

[8] T. Yu, Y. Shi, X. He, C. Kang, B. Deng, and S. Song, "Optimization of parameter ranges for composite tape winding process based on sensitivity analysis," *Appl. Compos. Mater.*, vol. 24, no. 4, pp. 821–836, Aug. 2017.

[9] L. Zu, H. Xu, B. Zhang, D. B. Li, H. B. Wang, and B. Zi, "Filament-wound composite sleeves of permanent magnet motor rotors with ultra-high fiber tension," *Compos. Struct.*, vol. 204, pp. 523–525, Nov. 2018.

[10] S. Eum, J. Lee, and K. Num, "Robust tension control of roll to roll winding equipment based on a disturbance observer," in *Proc. 42nd IECON*, Oct. 2016, pp. 625–630.

[11] R. C. Wang, Y. Sun, and X. Y. Xu, "Research of cone tension control system in film winding based on fuzzy-neural net-work," (in Chinese), *Control Instrum. Chem. Ind.*, vol. 40, no. 3, pp. 316–320, 2013.

[12] W. Y. Xie, X. Gao, S. Y. He, and X. H. Xiao, "Synergetic decoupling control of transport speed and tension for automated composite tape placement," (in Chinese), *Zhejiang Daxue Xuebao (Gongxue Ban)*, vol. 53, no. 3, pp. 455–462, 2019.

[13] Z. Wang, H. Nan, T. Shi, Q. Geng, and C. Xia, "No-tension sensor closed-loop control method with adaptive PI parameters for two-motor winding system," *Math. Problems Eng.*, vol. 2018, pp. 1–14, 2018.

[14] N. R. Abjadi, J. Askari, J. Soltani, and G. R. A. Markadeh, "Nonlinear sliding-mode control of a multi-motor Web-winding system without tension sensor," *IET Control Theory Appl.*, vol. 3, no. 4, pp. 419–427, Apr. 2009.

[15] H. Hou, X. Nian, J. Chen, and D. Xiao, "Decentralized coordinated control of elastic Web winding systems without tension sensor," *ISA Trans.*, vol. 80, pp. 350–359, Sep. 2018.

[16] K. C. Lin, M. C. Tsai, and K. Y. Chen, "Web tension control of a start-up process using observer techniques with friction and inertia compensation," in *Proc. 5th IECON*, Nov. 2001, pp. 529–534.

[17] D. Knittel, E. Laroche, D. Gigan, and H. Koc, "Tension control for winding systems with two-degrees-of-freedom H∞ controllers," *IEEE Trans. Ind. Appl.*, vol. 39, no. 1, pp. 113–120, Jan. 2003.

[18] Y. Shi, L. Yan, and X. He, "Variable tension control for discontinuous tape winding of composites based on constant extension ratio," *Chin. J. Mech. Eng.*, vol. 25, no. 5, pp. 1022–1028, Sep. 2012.

[19] A. Simorgh, A. Razminia, and V. I. Shiryaev, "System identification and control design of a nonlinear continuously stirred tank reactor," *Math. Comput. Simul.*, vol. 173, pp. 16–31, Jul. 2020.

[20] R. D. O. Pereira, M. Veronesi, A. Visioli, J. E. Normey-Rico, and B. C. Torrico, "Implementation and test of a new autotuning method for PID controllers of TITO processes," *Control Eng. Pract.*, vol. 58, pp. 171–185, Jan. 2017.

[21] M. Karami, A. R. Tavakolpour-Saleh, and A. Norouzi, "Optimal nonlinear PID control of a micro-robot equipped with vibratory actuator using ant colony algorithm: Simulation and experiment," *J. Intell. Robotic Syst.*, Feb. 2020.

[22] Y. P. Weng and X. W. Gao, "Data-driven sliding mode control of unknown MIMO nonlinear discrete-time systems with moving PID sliding surface," *J. Franklin Inst.*, vol. 354, no. 15, pp. 6463–6502, Oct. 2017.

[23] S. Sharifi, S. Ahmadyan, and S. Ebrahimi, "Designing of incorporating fuzzy-sliding mode controller based on strategy moving sliding surface for two-link robot manipulator," *J. Frankl. Inst.-Eng. Appl. Math.*, vol. 9, no. 4, pp. 3475–3480, 2012.

[24] I. M. Boiko, "Chattering in sliding mode control systems with boundary layer approximation of discontinuous control," *Int. J. Syst. Sci.*, vol. 44, no. 6, pp. 1–8, Jun. 2013.

[25] Y. Shtessel, C. Edwards, L. Fridman, and A. Levant, *Sliding Mode Control and Observation*. New York, NY, USA: Springer, 2014, pp. 163–166.

[26] F. F. M. El-Sousy, "Adaptive dynamic sliding-mode control system using recurrent RBFN for high-performance induction motor servo drive," *IEEE Trans. Ind. Informat.*, vol. 9, no. 4, pp. 1922–1936, Nov. 2013.

[27] J. Velasco, O. Barambones, I. Calvo, J. Zubia, I. Saez de Ocariz, and A. Chouza, "Sliding mode control with dynamical correction for time-delay piezoelectric actuator systems," *Materials*, vol. 13, no. 1, p. 132, Dec. 2019.

[28] Y. Zhao, W. Qiao, and L. Wu, "An adaptive Quasi-sliding-mode rotor position observer-based sensorless control for interior permanent magnet synchronous machines," *IEEE Trans. Power Electron.*, vol. 28, no. 12, pp. 5618–5629, Dec. 2013.

[29] C.-F. Huang, T.-L. Liao, C.-Y. Chen, and J.-J. Yan, "The design of quasi-sliding mode control for a permanent magnet synchronous motor with unmatched uncertainties," *Comput. Math. Appl.*, vol. 64, no. 5, pp. 1036–1043, Sep. 2012.

[30] A. Wang, X. Jia, and S. Dong, "A new exponential reaching law of sliding mode control to improve performance of permanent magnet synchronous motor," *IEEE Trans. Magn.*, vol. 49, no. 5, pp. 2409–2412, May 2013.

[31] C. Cheng, S. Liu, H. Wu, and Y. Zhang, "Neural network–based direct adaptive robust control of unknown MIMO nonlinear systems using state observer," *Int. J. Adapt. Control Signal Process.*, vol. 34, no. 1, pp. 1–14, Jan. 2020.

[32] J. He, M. Luo, Q. Zhang, J. Zhao, and L. Xu, "Adaptive fuzzy sliding mode controller with nonlinear observer for redundant manipulators handling varying external force," *J. Bionic Eng.*, vol. 13, no. 4, pp. 600–611, Dec. 2016.

[33] X. Sun, Z. Shi, L. Chen, and Z. Yang, "Internal model control for a bearingless permanent magnet synchronous motor based on inverse system method," *IEEE Trans. Energy Convers.*, vol. 31, no. 4, pp. 1539–1548, Dec. 2016.

[34] X. Sun, L. Chen, Z. Yang, and H. Zhu, "Speed-sensorless vector control of a bearingless induction motor with artificial neural network inverse speed observer," *IEEE/ASME Trans. Mechatronics*, vol. 18, no. 4, pp. 1357–1366, Aug. 2013.

[35] X. Sun, C. Hu, G. Lei, Y. Guo, and J. Zhu, "State feedback control for a PM hub motor based on gray wolf optimization algorithm," *IEEE Trans. Power Electron.*, vol. 35, no. 1, pp. 1136–1146, Jan. 2020.

[36] X. Sun, C. Hu, G. Lei, Z. Yang, Y. Guo, and J. Zhu, "Speed sensorless control of SPMSM drives for EVs with a binary search algorithm-based phase-locked loop," *IEEE Trans. Veh. Technol.*, vol. 69, no. 5, pp. 4968–4978, May 2020.

[37] X. Sun, J. Cao, G. Lei, Y. Guo, and J. Zhu, "Speed sensorless control for permanent magnet synchronous motors based on finite position set," *IEEE Trans. Ind. Electron.*, vol. 67, no. 7, pp. 6089–6100, Jul. 2020.

[38] Y.-J. Liu and N. Zhou, "Observer-based adaptive fuzzy-neural control for a class of uncertain nonlinear systems with unknown dead-zone input," *ISA Trans.*, vol. 49, no. 4, pp. 462–469, Oct. 2010.

[39] X. Shi and S. Chang, "Extended state observer-based time-optimal control for fast and precise point-to-point motions driven by a novel electromagnetic linear actuator," *Mechatronics*, vol. 23, no. 4, pp. 445–451, Jun. 2013.

[40] B.-Z. Guo and Z.-L. Zhao, "On the convergence of an extended state observer for nonlinear systems with uncertainty," *Syst. Control Lett.*, vol. 60, no. 6, pp. 420–430, Jun. 2011.

[41] S. E. Talole, J. P. Kolhe, and S. B. Phadke, "Extended-state-observer-based control of flexible-joint system with experimental validation," *IEEE Trans. Ind. Electron.*, vol. 57, no. 4, pp. 1411–1419, Apr. 2010.

[42] L. D. S. Coelho and M. A. B. Cunha, "Adaptive cascade control of a hydraulic actuator with an adaptive dead-zone compensation and optimization based on evolutionary algorithms," *Expert Syst. Appl.*, vol. 38, no. 10, pp. 12262–12269, Sep. 2011.

[43] S. Paciornik and J. d'Almeida, "Digital microscopy and image analysis applied to composite materials characterization," *Matéria (Rio de Janeiro)*, vol. 15, no. 2, pp. 172–181, 2010.

[44] B. Fedulov, F. Antonov, A. Safonov, A. Ushakov, and S. Lomov, "Influence of fibre misalignment and voids on composite laminate strength," *J. Compos. Mater.*, vol. 49, no. 23, pp. 2887–2896, Sep. 2015.

[45] K. Croft, L. Lessard, D. Pasini, M. Hojjati, J. Chen, and A. Yousefpour, "Experimental study of the effect of automated fiber placement induced defects on performance of composite laminates," *Compos. A, Appl. Sci. Manuf.*, vol. 42, no. 5, pp. 484–491, May 2011.

[46] T. Okuya, M. Nakada, and Y. Miyano, "Reliable test method for tensile strength in longitudinal direction of unidirectional carbon fiber-reinforced plastics," *J. Reinforced Plastics Composites*, vol. 32, no. 21, pp. 1579–1585, Nov. 2013.

[47] B. Deng and Y. Shi, "Modeling and simulation of voids in composite tape winding process based on domain superposition technique," *Appl. Compos. Mater.*, vol. 25, no. 5, pp. 1219–1236, Oct. 2018.

[48] S. Devanathan and P. N. Koch, "Comparison of Meta-Modeling Approaches for Optimization," in *Proc. IMECE*, Nov. 2011, pp. 827–835.

[49] *Standardization Administration of the People's Republic of China. Test Method for Mechanical Properties of Ring of Filament-Winding Reinforced Plastics*, Standard GT/B 1458-2008, Standardization Administration of the People's Republic of China, Beijing, China, 2008.

[50] S. Paciornik and J. R. M. D'Almeida, "Measurement of void content and distribution in composite materials through digital microscopy," *J. Compos. Mater.*, vol. 43, no. 2, pp. 101–112, Jan. 2009.

[51] H. Zhu, B. Wu, D. Li, D. Zhang, and Y. Chen, "Influence of voids on the tensile performance of carbon/epoxy fabric laminates," *J. Mater. Sci. Technol.*, vol. 27, no. 1, pp. 69–73, Jan. 2011.

[52] Y. Nikishkov, L. Airoldi, and A. Makeev, "Measurement of voids in composites by X-ray computed tomography," *Compos. Sci. Technol.*, vol. 89, pp. 89–97, Dec. 2013.

[53] *Carbon Fiber Reinforced Plastics–Determination of Void Content and Fiber Volume Content*, Standard GB/T 3365-2008, Standards of the People's Republic of China.

[54] J. W. Kim and D. G. Lee, "Measurement of residual stresses in thick composite cylinders by the radial-cut-cylinder-bending method," *Compos. Struct.*, vol. 77, no. 4, pp. 444–456, Feb. 2007.

[55] J. W. Kim, J. H. Lee, H. G. Kim, H. S. Kim, and D. G. Lee, "Reduction of residual stresses in thick-walled composite cylinders by smart cure cycle with cooling and reheating," *Compos. Struct.*, vol. 75, nos. 1–4, pp. 261–266, Sep. 2006.

YAOYAO SHI is currently a Professor with the School of Mechanical Engineering, Northwestern Polytechnic University. He is mainly involved in electromechanical control and automation, special CNC process equipment, high-speed and high-efficiency CNC machining, and the finishing technology of machining surfaces.

QI HONG received the B.S. degree from Nanchang Hangkong University, Nanchang, China, in 2013, and the M.S. degree from Northwestern Polytechnic University, Xi'an, China, in 2017, where he is currently pursuing the Ph.D. degree. His research interests include composite forming process and composite forming equipment.

ZHEN CHEN received the B.S. and M.S. degrees from Xi'an Polytechnic University, Xi'an, China, in 2013 and 2016, respectively. He is currently pursuing the Ph.D. degree with Northwestern Polytechnic University, Xi'an. His research interests include complex surface polishing technology and polishing equipment.

● ● ●